Numerical simulation of unsteady sheet/cloud cavitation

Numerical simulation of unsteady sheet/cloud cavitation

T D Tran[1], B Nennemann[2], T C Vu[2] and F Guibault[3]
[1] Department of Mechanical Engineering, École Polytechnique de Montréal Montreal, Quebec, Canada
[2] Andritz-Hydro Ltd., Montreal, Quebec, Canada
[3] Department of Computer and Software Engineering, École Polytechnique de Montréal, Montreal, Quebec, Canada

E-mail: tan-dung.tran@polymtl.ca

Abstract. Unsteady Reynolds-averaged Navier-Stokes (URANS) coupling with mass transfer cavitation models was used to resolve the turbulent flow structure with cavitation. Kubota and Merkle cavitation models were tested. As part of the work, the Merkle model is implemented into CFX by User Fortran code because this model has shown good cavitation prediction capability according to the literature. The results will focus on the unsteady cavitation shedding dynamics around NACA66 hydrofoil. The predicted results compare well with the experimental measurements for unsteady sheet/cloud cavitating flows. Numerical visualizations of cloud cavity evolution and surface pressure signals show relatively good agreement with the experimental data.

1. Introduction

The goal of this project is to predict the pressure fluctuations in hydraulic turbines by numerical modelling. Cavitation is a major contributing factor to pressure fluctuations, characterized by their amplitude and frequency, in hydraulic turbines. They can lead to unwanted noise, vibrations and material fatigue issues. Consequently, the ability to simulate cavitation with reasonable accuracy is of high importance regarding the prediction of dynamic loads that act on the turbine components under these pressure fluctuations. In order to better understand the prediction quality of various existing cavitation models, it is useful to study them on a geometrically simple case with well-documented, high-quality measurement data for validation.

The cavitation phenomenon often involves complex interactions between turbulent flow structures and phase-change dynamics with large variations in fluid density and pressure fluctuations [1]. These physical mechanisms are still not well understood because of the complex, multi-scale, multiphase phenomenon. In the past decades, lots of research, including experiments and simulations, was conducted to understand the mechanism of unsteady cavitation shedding. Moreover, there are significant computational challenges associated with the accuracy, stability, efficiency, and robustness of numerical algorithms for the simulation of turbulent cavitating flows.

In the numerical modelling of cavitating flows, the selection of cavitation model plays a major role in the prediction of cavitation dynamics. In recent years, significant efforts have been made in the development of cavitation models; examples of recent review articles can be found in [2-4]. Many cavitation models have been based on the assumption of a homogenous equilibrium medium proposed by Kubota et al. [5], where the slip between the liquid and vapour interface is neglected and the liquid-

vapour mixture is treated as a single fluid that satisfies the Navier-Stokes equations. A key point in this kind of model is how to define the mixture density. There are two approaches:

- One approach is based on the state equation. Delannoy and Kueny used a barotropic state equation that linked the mixture density to the local static pressure $\rho_m = f(p)$. Coutier-Delgosha et al. [3] used a similar barotropic state equation together with a modified turbulent viscosity to successfully simulate cloud cavity shedding in a Venturi-type duct. A recent experimental finding by Gopalan et al. [6] has shown that vorticity production is an important aspect of cavitating flows, especially in the cavity closure region. Specifically, this vorticity production is a consequence of the baroclinic torque:

$$\nabla \frac{1}{\rho_m} \times \nabla p \tag{1}$$

  If a barotropic equation of state, $\rho_m = f(p)$, is used, the gradients of density and pressure are always parallel, which leads to zero baroclinic torque. Hence, barotropic cavitation models will not be able to properly predict the dynamics of cavitating flows [7].
- The other popular approach to simulate cavitating flows is transport equation models (TEMs), which solve an additional transport equation for either the mass or volume fraction of vapor, with appropriate source/sink term(s) to regulate the mass transfer between the liquid and vapor phases.
  - Different source/sink terms have been proposed, including the popular models presented in [5, 8, 9]. Kubota et al. [5] coupled the Rayleigh-Plesset equation with the RANS equations to solve for the local void fraction based on an assumed bubble radius. Merkle et al. [10] and Kunz et al. [8] employed the artificial compressibility method with a special preconditioning formulation to solve the multiphase RANS equations, comprised of the mixture volume, mixture momentum, and constituent volume fraction equations. Singhal et al. [9] developed a "full-cavitation model" based on the phase-change rate derived from a reduced form of the Rayleigh-Plesset equation for bubble dynamics and local flow conditions. Senocak and Shyy [11] compared different TEM models to develop an interfacial dynamics-based cavitation model (IDM), which allows direct interpretation of the empirical parameters in existing transport equation-based models. In the TEM approach, the mixture density is a function of the transport process. Consequently, gradients of the density and the pressure are not necessarily parallel, suggesting that TEM can accommodate baroclinic vorticity generation.

The objective of this paper is to evaluate the applicability of two cavitation models and determine appropriate numerical parameters for unsteady sheet/cloud cavitating flows in order to predict pressure fluctuations around a hydrofoil. The aim is to understand the influence of cavitating multiphase flow on cavity dynamics, and hydrodynamic performance. The simulations are performed for a NACA66 foil at 6 degrees angle of attack, Reynolds number of 750 000 and for a cavitation number corresponding to unsteady sheet/cloud cavitating regime. The incompressible, multiphase unsteady Reynolds-averaged Navier-Stokes (URANS) equations are solved by the CFD solver CFX with Kubota and Merkle cavitation models.

As part of the work, the Merkle model is implemented into CFX by User Fortran code because this model has shown good cavitation prediction capability according to the literature [12-16]. The Kubota model is the only default cavitation model in CFX. The Kubota model is also implemented into CFX by User Fortran code for methodology validation purposes.

The numerical models are first presented. The cavitation models Kubota, Merkle and the turbulence models k-ε are shown, followed by the presentation of the density correction model for the turbulent viscosity modification. The foil geometry, fluid mesh, and boundary conditions are presented, followed by a brief summary of the experimental setup of [17] used for validation of the computations. The results are then analysed for a NACA 66 hydrofoil at a fixed angle of incidence (α

= 6°) and Reynolds number (Re = 750 000) for a case with unsteady sheet/cloud cavitation (σ = 1.00). Numerical simulations of the cavitation development, cavity shedding and collapse are carried out. The results are compared with experimental data to analyse cavitation shedding dynamics.

2. Transport-based cavitation models

2.1. Conservation of mass and momentum

The unsteady RANS equations are believed to be adequate to model the quasi-steady sheet cavitation case studied here. These unsteady RANS equations, in their conservative form, for a Newtonian fluid without body forces and heat transfers, are presented below along with the mass transport equation in the Cartesian coordinates [18]:

$$\frac{\partial \rho_m}{\partial t} + \frac{\partial (\rho_m u_j)}{\partial x_j} = 0 \tag{2}$$

$$\frac{\partial (\rho_m u_i)}{\partial t} + \frac{\partial \left(\rho_m u_i u_j\right)}{\partial x_j} = -\frac{\partial p}{\partial x_i} + \frac{\partial}{\partial x_j}\left[(\mu_m + \mu_T)\left(\frac{\partial u_i}{\partial x_j} + \frac{\partial u_j}{\partial x_i} - \frac{2}{3}\frac{\partial u_k}{\partial x_k}\delta_{ij}\right)\right] \tag{3}$$

$$\frac{\partial (\rho_l \alpha_l u_j)}{\partial x_j} = -(\dot{m}^+ + \dot{m}^-) \tag{4}$$

$$\rho_m = \rho_l \alpha_l + \rho_v \alpha_v \tag{5}$$

$$\mu_m = \mu_l \alpha_l + \mu_v \alpha_v \tag{6}$$

where ρ_m is the mixture density, ρ_l is the liquid density, ρ_v is the vapor density, α_v is the vapor fraction, α_l is the liquid fraction, u is the velocity, p is the pressure, μ_m is the mixture laminar viscosity, μ_l and μ_v are, respectively, the liquid and vapor dynamic viscosities, and μ_T is the turbulent viscosity. The subscripts (i, j, and k) denote the directions of the Cartesian coordinates. The source term $\dot{m}^+$ and the sink term $\dot{m}^-$ represent the condensation and evaporation rates, respectively.

2.2. Kubota model

The Kubota model is sometimes called Zwart-Gerber-Belamri model or Rayleigh Plesset model. The Kubota model [5] assumes a constant nuclei density in the fluid domain. The growth and collapse of the bubble clusters are governed by the simplified Rayleigh-Plesset equation for single-bubble dynamics [19]. The cavitation process is governed by the mass transfer equation given in (4), and the source and sink terms are defined as follows:

$$\dot{m}^- = -C_{k\_dest}\frac{3\alpha_{nuc}(1-\alpha_v)\rho_v}{R_B}\left(\frac{2}{3}\frac{p_v - p}{\rho_l}\right)^{1/2}, p < p_v \tag{7}$$

$$\dot{m}^+ = C_{k\_prod}\frac{3\alpha_v \rho_v}{R_B}\left(\frac{2}{3}\frac{p - p_v}{\rho_l}\right)^{1/2}, p > p_v \tag{8}$$

where α_{nuc} is the nucleation volume fraction, R_B is the bubble diameter, p_v is the saturated liquid vapor pressure, and p is the local fluid pressure. C_{k_dest} is the rate constant for vapor generated from the

liquid in a region where the local pressure is less than the vapor pressure. Conversely, C_{k_prod} is the rate constant for reconversion of vapor back into liquid in regions where the local pressure exceeds the vapor pressure. As shown in (7) and (8), both the evaporation and condensation terms are assumed to be proportional to the square root of the difference between the local pressure and vapor pressure because the Kubota model was derived by assuming that the bubble dynamics are governed by the simplified Rayleigh-Plesset equation [19]. In this work, the assumed values for the model constants are $\alpha_{nuc} = 5 \times 10^{-4}$, $R_B = 1 \times 10^{-6}$ m, $C_{k\_dest} = 50$, and $C_{k\_prod} = 0.01$, which are the default values in CFX [20] and are used because of their claimed general applicability.

2.3. Merkle model

The Merkle model is sometimes called Kunz et al. model. Several researchers have adopted the Merkle model proposed by [10] (e.g., see [7], [12-16]), which has been presented in both the volume fraction form and the mass fraction form. It was derived primarily based on dimensional arguments for large-bubble clusters instead of individual bubbles. Consequently, the source and sink terms for the Merkle model shown in (9) are directly related to the pressure difference, $p - p_v$, instead of the square root of the pressure difference as in the Kubota model:

$$\dot{m}^- = \frac{C_{k\_dest}\rho_l\rho_l MIN(p-\rho_v, 0)(1-\alpha_v)}{(0.5\rho_l U_\infty^2)\rho_v t_\infty}, p < p_v \tag{9}$$

$$\dot{m}^+ = \frac{C_{m\_prod}\rho_l MAX(p-\rho_v, 0)\alpha_v}{(0.5\rho_l U_\infty^2)t_\infty}, p > p_v \tag{10}$$

In this work, the empirical factors are set to be $C_{m\_dest} = 1$ and $C_{m\_prod} = 80$, which follows the constants used by Senocak and Shyy [11] for simulation of quasi-steady cavitation around a NACA 66(MOD) hydrofoil. The mean flow time scale is defined as $t_\infty = c/U_\infty$ [7, 11] where c is the hydrofoil cord, U_∞ is equal to the inlet velocity.

As part of the present work, the Merkle model is implemented into CFX by User Fortran code. The Kubota model is also implemented by User Fortran code and its results are compared to the default model results in order to validate our implementation methodology.

2.4. Turbulence Models and Turbulence Viscosity Modification

The numerical simulations presented in this paper are performed using the commercial CFD code, CFX, to solve the RANS equations. The k-ε turbulence model is used.

It should be noted that the original RANS models were developed for fully incompressible single-phase flows and were not intended for flow problems involving compressible multiphase mixtures. To improve numerical simulations by taking into account the influence of the local compressibility effect of two-phase mixtures on turbulent closure models, Coutier-Delgosha [21] proposed to reduce the mixture turbulent viscosity based on the local liquid volume fraction α_l by substituting μ_T in (3) with μ_{T_mod}:

$$f(n) = \frac{\rho_v + (1-\alpha_v)^n(\rho_l - \rho_v)}{\rho_v + (1-\alpha_v)(\rho_l - \rho_v)}, \mu_{T\_mod} = \mu_T f(n) \tag{11}$$

The variation of the modified effective density, $\rho_m f(n)$, with the vapor volume fraction, α_v, for different values of n is shown in Figure 1.

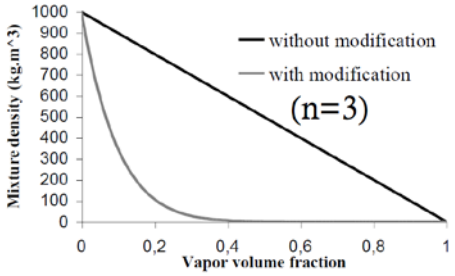

Figure 1. Local compresseibility modification of the mixture density according to (11)

In [12-16], it is recommended to use n = 3 to simulate the reentrant jet behavior and vapor shedding process for the simulation of cavitating flow around a hydrofoil, because they obtained favorable agreement between numerical and experimental results for this n = 3.

3. Experimental Setup and Description

To evaluate the predictive capabilities of the two different cavitation models with different local compressibility corrections, numerical computations are compared with experimental measurements of the NACA 66 hydrofoil conducted at the cavitation tunnel at the Research Institute of the French Naval Academy. The test section has a cross-sectional area of 0.192 m^2 and length of 1 m. The inflow velocity ranges between 3 m/s and 15 m/s, and the pressure in the test section ranges between 30 mbar and 3 bars. The tunnel inflow turbulence intensity, defined as $V_{\infty rms}/V_{\infty}$ at the inlet of the test section, is about 2%. The foil has a uniform cross-section with a NACA 66 thickness distribution with a maximum thickness-to-chord ratio of 12%, and a = 0.8 camber distribution with a maximum camber-to-chord ratio of 2%. The chord length is c = 0.15 m and the span length is s = 0.191 m. The hydrofoil is made of stainless steel, and behaved like a 2D rigid hydrofoil even though it was mounted using a cantilevered setup with a small gap (1 mm) between the free end of the hydrofoil and the test section wall.

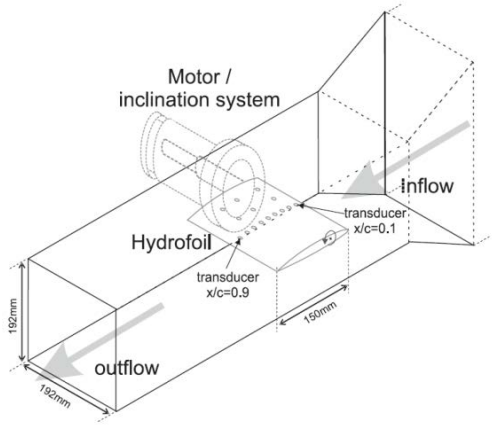

Figure 2. Hydrofoil instrumentation and tunnel test section [22]

Pressure measurements were carried out using seventeen flush-mounted piezo-resistive transducers with a maximum pressure of 10 bars. The transducer locations were aligned along the chord on the suction side of the hydrofoil at mid-span, starting from the foil leading edge at a reduced coordinate of x/c = 0.1 to the trailing edge at x/c = 0.9, with increments of 0.1 c. Therefore, the possible tip-vortex cavitation caused by the small gap between the hydrofoil end and the wall could not have significant influence on the mid-span section. Lift and drag were measured using a resistive gauge hydrodynamic balance with a range up to 1500 N in lift and 150 N in drag. Readers should refer to [17, 23] for additional details about the rigid hydrofoil experimental setup and results. The experimental results presented in this paper are taken from [17] for cases with unsteady sheet/cloud cavitation.

4. Numerical Setup and Description

To demonstrate and validate the numerical model, results are shown for the rigid rectangular NACA 66 hydrofoil described above. All the results shown in this paper correspond to the hydrofoil fixed at $\alpha = 6°$ and subject to a nominal free stream velocity of $V_\infty = 5$ m/s, which yields a moderate-to-high Reynolds number of $Re = V_\infty c/\nu_l = 0.75 \times 10^6$.

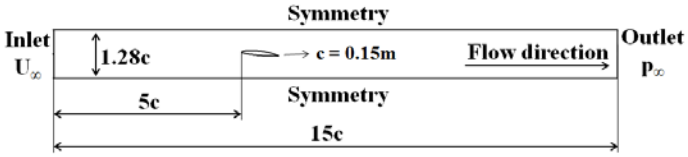

Figure 3. Fluid domain and boundary conditions

The density and dynamic viscosities of the liquid are taken to be $\rho_l = 999.19$ kg/m^3 and $\mu_l = \rho_l \nu_l = 1.139 \times 10^{-3}$ Pa·s, respectively, which correspond to fresh water at 25°C. The vapor density is $\rho_v = 0.02308$ kg/m^3 and the vapor viscosity is $\mu_v = 9.8626 \times 10^{-6}$ Pa·s. The vapor pressure of water at 25°C is $p_v = 3169$ Pa.

Based on the experimental observations of cavitating flow over the 3D rectangular hydrofoil [24], the flow is found to be approximately uniform over 80 to 90% of the foil. Hence, for computational efficiency, the 2D analysis is applied in this work. The 2D fluid domain is shown in Figure 3, which corresponds to the height of the experimental test section at the French Naval Academy. The computational domain has an extent of about 5 c upstream and 10 c downstream of the foil to simulate near-infinite boundary conditions at the inlet and outlet. Although the boundary layer growth may affect the flow at the foil and the turbulence intensity may change to a different extend if the inlet is too far, the inlet cannot be set at the same distance upstream as the experiment because the exact parabolic velocity profile cannot be found in the experimental papers. A no-slip boundary condition is imposed on the hydrofoil surface. The symmetry conditions are imposed on the top and bottom boundaries of the tunnel because our tested simulations with the symmetry conditions and the wall conditions on these boundaries gave the same results for this case. Moreover, the use of the symmetry conditions allows to do not concentrate the mesh near the top and the bottom in order to optimize the mesh and the simulation time. The inlet velocity is set to be $V_\infty = 5$m/s and the outlet pressure is set to vary according to the cavitation number, defined as $\sigma = (p_\infty - p_v)/(0.5\rho_l V_\infty^2)$, where p_∞ is the tunnel pressure. This p_∞ is used to set the pressure outlet boundary condition. A constant turbulent intensity of 2% is set at the inlet boundary and is equal to the experimentally measured turbulent intensity.

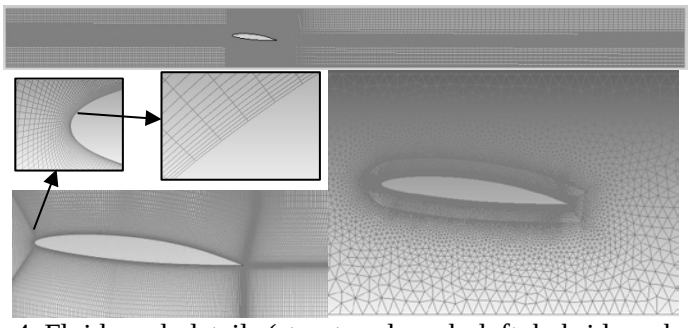

Figure 4. Fluid mesh details (structured mesh: left, hybrid mesh: right)

All cavitating runs have been initialized with a fully wetted simulation or no-cavitation simulation to avoid any vapor fraction. The tunnel pressure is then decreased progressively until the particular cavitation number is reached. Fully structured meshes generated by ICEM are composed of 124000 nodes and 98000 nodes corresponding to $y^+ = 1$ and 3 where $y^+ = yu_\tau/\nu_l$, y is the thickness of the first cell from the foil surface, and u_τ is the wall frictional velocity. Hybrid meshes generated by our in-

house mesh generator are composed of 70000 nodes with 50 structured nodes across the foil boundary layer, which is selected to ensure $y^+ = 1$. In the hybrid meshes, the regions outside the boundary layer have been discretized with unstructured triangular elements. Mesh refinements are performed at the foil leading edge, trailing edge, and in the wake region. The spatial derivatives are computed using a second-order upwind scheme. The time integration scheme is a second-order backward Euler algorithm, and the spatial derivatives are computed using a second-order upwind scheme. The influence of mesh concentration has been studied also for this case with the hybrid mesh for different mesh concentration zones.

The effects of turbulence models, mesh types, and mesh concentrations on the cavitating flow dynamics have been studied in detail for the case of the rigid NACA 66 hydrofoil at a fixed angle of attack of $\alpha = 6°$ in steady flow for the quasi-steady sheet cavitating case ($\sigma = 1.49$), Re = 750 000; see [25] for more details. Our previous work has shown that the k-ε model has given better results than SST turbulence model for this case study. The hydrid meshes have performed very well for these cavitating simulations, giving almost the same results as structured meshes. Therefore, in this paper, only the simulation results using structured meshes and k-ε turbulence model will be presented.

5. Results:

5.1. Prediction of the pressure fluctuations on the hydrofoil

To evaluate the predictability of the three different cavitation models for unsteady sheet/cloud cavitation, results are shown for the case with $\sigma = 1.00$, Re = 750 000, $\alpha = 6°$ and with the timestep $\Delta t = 1\times10^{-2}$ s.

Based on available experimental data presented in [23], an analysis of suction side loading can be calculated by summing the pressure coefficients along the suction side, which was calculated as follows in the experimental study:

$$C_l^+(t) = \sum_{i=1}^{10} C_P\left(\frac{x_i}{c,t}\right)\Delta\left(\frac{x_i}{c}\right) \tag{12}$$

where $C_P(x_i/c,t)$ is the pressure coefficient at location x_i/c and $\Delta(x_i/c) = 0.1$ is the non-dimensional distance between two consecutive pressure transducers. For comparison purposes, the same procedure is applied to calculate the numerically derived suction side lift coefficient. It should be noted that since the flow is mostly attached along the pressure side, the changes to the total lift coefficient should be dominated by the suction side dynamics, which is represented by the suction side lift coefficient.

Comparisons of the predicted and measured suction side lift coefficients are shown in Figure 5. A fair comparison is observed between the experimental measurements and numerical predictions obtained with both the Kubota and the Merkle model. The maximum, minimum, and mean values of the suction side lift coefficient predicted using the two cavitation models are in quite good agreement with experiments.

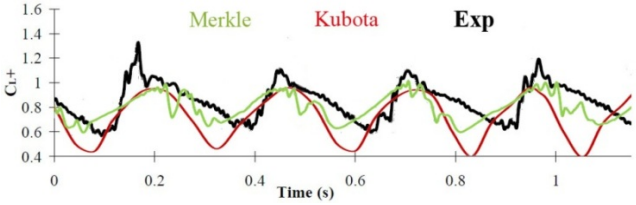

Figure 5. Comparisons of the measured and the predicted suction side lift coefficients obtained using the Kubota cavitation model and Merkle cavitation model

5.2. Prediction of cavitation vapor on the hydrofoil

Vapor fraction Kubota Model (a)	Vapor fraction Merkle Model (b)	Experiments (c)
		
	t_1 = 20% Cycle	
		
	t_2 = 36% Cycle	
		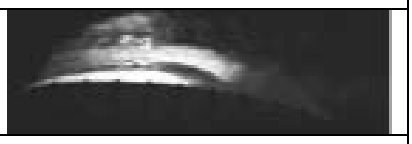
	t_3 = 52% Cycle	
		
	t_4 = 60% Cycle	
		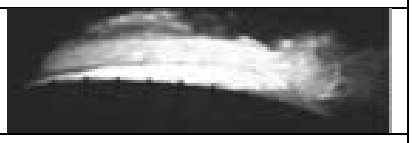
	t_5 = 68% Cycle	
		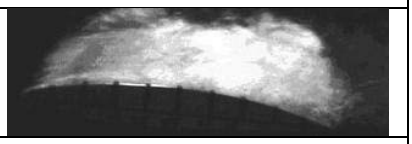
	t_6 = 76% Cycle	
		
	t_7 = 84% Cycle	

Figure 6. Comparisons of the predicted vapour fraction contours predicted using the Kubota and Merkle cavitation model with experimental observations

Figure 6 shows the comparisons between the predicted vapor fraction obtained using the Kubota and the Merkle models with experimental visualizations presented in [23] for the operating condition σ = 1.00, Re = 750 000, α = 6°. The predicted cavity behavior obtained using the Merkle model is generally in better agreement with the experiments than the Kubota model. As shown in Figure 6, a stable leading edge sheet cavity gradually expands toward the foil trailing edge between times t_1 to t_3. The upstream motion of the re-entrant jet can be observed at times t_3 and t_4 in Figure 6 (a and b). The clockwise vorticity generated by the re-entrant jet causes the cavity to roll up and partially sheds at times t_4 and t_5 and is supported by the foamy appearance of the cavity trailing edge in Figure 6 (c). At time t_6, the sheet cavity mostly sheds; the cavity flows downstream and forms a cloud cavity, which can be seen at time t_7.

5.3. Effect of the turbulent viscosity

For the Kubota model, without turbulence viscosity modification (n = 1), the cavity shedding frequency is approximately 4.1 Hz, as shown in Table 1. With turbulence viscosity modification (n = 3), the frequency is changed to be around 3.6 Hz which is closer to the measured value.

Similarly, for the Merkle model, without turbulence viscosity modification (n = 1), the cavity shedding frequency is approximately 3.9 Hz, as shown in Table 1. With turbulence viscosity modification (n = 3), the frequency is changed to be around 3.4 Hz which is closer to the measured value.

Table 1 Comparison of the measures and predicted cavity shedding frequencies for the Kubota and Merkle cavitation models with n = 1 and n = 3 for the case of unsteady sheet/cloud cavitation

	Kubota model		Merkle model		Experiments
	No turbulence viscosity modification (n = 1)	With turbulence viscosity modification (n = 3)	No turbulence viscosity modification (n = 1)	With turbulence viscosity modification (n = 3)	
Shedding frequency (Hz)	4.1	3.6	3.9	3.4	3.5

6. Conclusions

The applicability of two popular transport-based cavitation models is compared for the simulation of cavitating flow around a NACA66 hydrofoil at Re = 750 000. The effect of local compressibility is considered with a turbulent viscosity modification. Results are shown for unsteady sheet/cloud cavitation $\sigma = 1.00$) around the hydrofoil fixed at $\alpha = 6°$. Both the amplitude and frequency of the suction side lift coefficient predicted using the Kubota and Merkle models agreed well with experimental measurements. Good comparisons were also observed between predicted cavitation patterns obtained using the tested cavitation models and experimental visualizations.

The fact of adding the Merkle cavitation model by User Fortran code makes the numeric convergence to be very difficult, especially for this complex unsteady sheet/cloud shedding cavitation. Please note that the modification of turbulence viscosity makes the simulation also harder to converge. Generally, the convergence is better with bigger timestep than smaller timestep. This numeric problem would need more efforts to improve the convergence in the future. Additional systematic validation studies are currently underway.

7. References

[1] Tseng, C-C, and Shyy, W, 2010, "Modeling for isothermal and cryogenic cavitation," International Journal of Heat and Mass Transfer, **53**(1-3), pp. 513-525

[2] Morgut, M, Nobile, E, and Bilus, I, 2011, "Comparison of mass transfer models for the numerical prediction of sheet cavitation around a hydrofoil," International Journal of Multiphase Flow, **37**(6), pp. 620-626.

[3] Arndt, R E A, 2012, "Some remarks on hydrofoil cavitation," Journal of Hydrodynamics, **24**(3), pp. 305-314

[4] Arndt, R E A, "Cavitation research from an intetrnational perspective," Proc. 26th IAHR Symposium on Hydraulic Machinery and Systems, August 19, 2012 - August 23, 2012, Institute of Physics Publishing

[5] Kubota, A, Kato, H, and Yamaguchi, H, 1992, "A new modelling of cavitating flows: a numerical study of unsteady cavitation on a hydrofoil section," Journal of Fluid Mechanics, **240**, pp. 59-96

[6] Gopalan, S, and Katz, J, 2000, "Flow structure and modeling issues in the closure region of attached cavitation," Physics of Fluids, **12**(4), pp. 895-911

[7] Senocak, I, and Shyy, W, "Evaluation of cavitation models for Navier-Stokes computations," Proc. Proceedings of the 2002 ASME Joint U.S.-European Fluids Engineering Conference, July 14, 2002 - July 18, 2002, American Society of Mechanical Engineers, pp. 395-401

[8] Kunz, R F, Boger, D A, Stinebring, D R, Chyczewski, T S, Lindau, J W, Gibeling, H J, Venkateswaran, S, and Govindan, T R, 2000, "A preconditioned Navier-Stokes method for two-phase flows with application to cavitation prediction," Computers & Fluids, **29**(8), pp. 849-875
[9] Singhal, A K, Athavale, M M, Huiying, L, and Yu, J, 2002, "Mathematical basis and validation of the full cavitation model," Transactions of the ASME. Journal of Fluids Engineering, **124**(3), pp. 617-624
[10] Merkle, C L, Feng, J Z, and Buelow, P E O, "Computational modeling of the dynamics of sheet cavitation," Proc. Proceedings of the 3rd International Symposium on Cavitation
[11] Senocak, I, and Shyy, W, 2002, "A Pressure-Based Method for Turbulent Cavitating Flow Computations," Journal of Computational Physics, **176**(2), pp. 363-383
[12] Ducoin, A, Huang, B, and Young, Y L, 2012, "Numerical Modeling of Unsteady Cavitating Flows around a Stationary Hydrofoil," International Journal of Rotating Machinery, 2012, pp. 1-17
[13] Huang, B, Ducoin, A, and Young, Y L, "Evaluation of Cavitation Models for Prediction of Transient Cavitating Flows around a Stationary and a Pitching Hydrofoil," Proc. 8th International Symposium on Cavitation
[14] Young, Y L J, Chae, E J, Akcabay, D, Biao, H, and Ducoin, A, 2012-08, "Fluid-Structure Interaction Response & Stability of Hydrofoils," 26th IAHR Symposium on Hydraulic Machinery and Systems, Beijing, China
[15] Huang, B, Ducoin, A, and Young, Y L, 2013, "Physical and numerical investigation of cavitating flows around a pitching hydrofoil," Physics of Fluids, **25**(10)
[16] Huang, B, Young, Y L, Wang, G, and Shyy, W, 2013, "Combined Experimental and Computational Investigation of Unsteady Structure of Sheet/Cloud Cavitation," Journal of Fluids Engineering, **135**(7), pp. 071301-071301
[17] Leroux, J.-B, Astolfi, J A, and Billard, J Y, 2004, "An experimental study of unsteady partial cavitation," Journal of Fluids Engineering, Transactions of the ASME, **126**(1), pp. 94-101
[18] Launder, B E, and Spalding, D B, 1974, "The numerical computation of turbulent flows," Computer Methods in Applied Mechanics and Engineering, **3**(2), pp. 269-289
[19] Brennen, C E, 2005, Fundamentals of Multiphase Flow, Cambridge University Press
[20] ANSYS, 2012-10, "ANSYS CFX Tutorials 14.5."
[21] Coutier-Delgosha, O, Fortes-Patella, R, and Reboud, J L, 2003, "Evaluation of the turbulence model influence on the numerical simulations of unsteady cavitation," Journal of Fluids Engineering, Transactions of the ASME, **125**(1), pp. 38-45
[22] Ducoin, A, Astolfi, J A, Deniset, F, and Sigrist, J F, 2009, "Computational and experimental investigation of flow over a transient pitching hydrofoil," European Journal of Mechanics, B/Fluids, **28**(6), pp. 728-743
[23] Leroux, J-B, Coutier-Delgosha, O, and Astolfi, J A, 2005, "A joint experimental and numerical study of mechanisms associated to instability of partial cavitation on two-dimensional hydrofoil," Physics of Fluids, **17**(5), pp. 1-20
[24] Wang, G, Senocak, I, Shyy, W, Ikohagi, T, and Cao, S, 2001, "Dynamics of attached turbulent cavitating flows," Progress in Aerospace Sciences, **37**(6), pp. 551-581
[25] Tran, T D, Nennemann, B, Vu, T C, and Guibault, F, "Numerical Simulation of Cavitating Flow around a Hydrofoil," Proc. Proceedings of the ASME 2014 4th Joint US-European Fluids Engineering Division Summer; 49th Forum on Cavitation and Multiphase Flow